Analysis of Ge micro-cavities with in-plane tensile strains above 2 %

R.W. Millar,[1] K. Gallacher,[1] J. Frigerio,[2] A. Ballabio,[2] A. Bashir,[3] I. MacLaren,[3] G. Isella,[2] and D. J. Paul[1,*]

[1]*School of Engineering, University of Glasgow, Rankine Building, Oakfield Avenue, Glasgow, G12 8LT, UK*
[2]*L-NESS, Politecnico di Milano, Via Anzani 42, 22100, Como, Italy*
[3]*School of Physics and Astronomy, University of Glasgow, Kelvin Building, Glasgow, G12 8QQ, UK*
[*]*Douglas.Paul@glasgow.ac.uk*

Abstract: Ge on Si micro-disk, ring and racetrack cavities are fabricated and strained using silicon nitride stressor layers. Photoluminescence measurements demonstrate emission at wavelengths $\geq$ 2.3 μm, and the highest strained samples demonstrate in-plane, tensile strains of $>$ 2 %, as measured by Raman spectroscopy. Strain analysis of the micro-disk structures demonstrate that shear strains are present in circular cavities, which can detrimentally effect the carrier concentration for direct band transitions. The advantages and disadvantages of each type of proposed cavity structure are discussed.

OCIS codes: (130.3130) Integrated optics materials; (130.5990) Semiconductors; (130.3120) Integrated optics devices; (130.3060) Infrared.

References and links

1. D. J. Paul, "8-band **k**.**p** modeling of the quantum confined Stark effect in Ge quantum wells on Si substrates," Phys. Rev. B **77**, 155323 (2008).
2. R. Soref, "Mid-infrared photonics in silicon and germanium," Nat. Photonics **4**, 495–497 (2010).
3. D. J. Paul, "The progress towards terahertz quantum cascade lasers on silicon substrates," Laser Photonics Rev. **4**, 610–632 (2010).
4. L. Baldassarre, E. Sakat, J. Frigerio, A. Samarelli, K. Gallacher, E. Calandrini, G. Isella, D. J. Paul, M. Ortolani, and P. Biagioni, "Midinfrared plasmon-enhanced spectroscopy with germanium antennas on silicon substrates," Nano Lett. **15**, 7225–7231 (2015).
5. D. J. Paul, "Silicon photonics: a bright future?" Electron. Lett. **45**, 582–584 (2009).
6. M. Prost, M. El Kurdi, F. Aniel, N. Zerounian, S. Sauvage, X. Checoury, F. Bœuf, and P. Boucaud, "Analysis of optical gain threshold in n-doped and tensile-strained germanium heterostructure diodes," J. Appl. Phys. **118**, 125704 (2015).
7. J. Liu, X. Sun, R. Camacho-Aguilera, L. C. Kimerling, and J. Michel, "Ge-on-Si laser operating at room temperature,," Opt. Lett. **35**, 679–681 (2010).
8. R. E. Camacho-Aguilera, Y. Cai, N. Patel, J. T. Bessette, M. Romagnoli, L. C. Kimerling, and J. Michel, "An electrically pumped germanium laser,," Opt. Express **20**, 11316–20 (2012).
9. J. R. Sanchez-Perez, C. Boztug, F. Chen, F. F. Sudradjat, D. M. Paskiewicz, R. Jacobson, M. G. Lagally, and R. Paiella, "Direct-bandgap light-emitting germanium in tensilely strained nanomembranes," Proc. Nat. Acad. Sci. **108**, 18893–18898 (2011).
10. S. Wirths, R. Geiger, N. von den Driesch, G. Mussler, T. Stoica, S. Mantl, Z. Ikonic, M. Luysberg, S. Chiussi, J. M. Hartmann, H. Sigg, J. Faist, D. Buca, and D. Grützmacher, "Lasing in direct-bandgap GeSn alloy grown on Si," Nat. Photonics **9**, 88–92 (2015).
11. M. J. Suess, R. Geiger, R. A. Minamisawa, G. Schiefler, J. Frigerio, D. Chrastina, G. Isella, R. Spolenak, J. Faist, and H. Sigg, "Analysis of enhanced light emission from highly strained germanium microbridges," Nat. Photonics **7**, 466–472 (2013).

#255977 Received 16 Dec 2015; revised 14 Feb 2016; accepted 14 Feb 2016; published 22 Feb 2016

12. G. Capellini, C. Reich, S. Guha, Y. Yamamoto, M. Lisker, M. Virgilio, A. Ghrib, M. E. Kurdi, P. Boucaud, B. Tillack, and T. Schroeder, "Tensile Ge microstructures for lasing fabricated by means of a silicon complementary metal-oxide-semiconductor process," Opt. Express **22**, 399–410 (2014).
13. R. W. Millar, K. Gallacher, A. Samarelli, J. Frigerio, D. Chrastina, G. Isella, T. Dieing, and D. J. Paul, "Extending the emission wavelength of Ge nanopillars to 2.25 μm using silicon nitride stressors," Opt. Express **23**, 18193–18202 (2015).
14. A. Ghrib, M. El Kurdi, M. de Kersauson, M. Prost, S. Sauvage, X. Checoury, G. Beaudoin, I. Sagnes, and P. Boucaud, "Tensile-strained germanium microdisks," Appl. Phys. Lett. **102**, 221112 (2013).
15. A. Ghrib, M. El Kurdi, M. Prost, S. Sauvage, X. Checoury, G. Beaudoin, M. Chaigneau, R. Ossikovski, I. Sagnes, and P. Boucaud, "All-around SiN stressor for high and homogeneous tensile strain in germanium microdisk cavities," Advanced Optical Materials **3**, 353–358 (2015).
16. A. Z. Al-Attili, S. Kako, M. Husain, F. Gardes, N. Higashitarumizu, S. Iwamoto, Y. Arakawa, Y. Ishikawa, H. Arimoto, K. Oda, T. Ido, and S. Saito, "Whispering gallery mode resonances from ge micro-disks on suspended beams," Frontiers in Materials **2** (2015).
17. R. Geiger, J. Frigerio, M. J. Süess, D. Chrastina, G. Isella, R. Spolenak, J. Faist, and H. Sigg, "Excess carrier lifetimes in Ge layers on Si," Appl. Phys. Lett. **104**, 062106 (2014).
18. M. M. Mirza, H. Zhou, P. Velha, X. Li, K. E. Docherty, A. Samarelli, G. Ternent, and D. J. Paul, "Nanofabrication of high aspect ratio (∼50:1) sub-10 nm silicon nanowires using inductively coupled plasma etching," J. Vac. Sci. Technol. B **30**, 06FF02 (2012).
19. M. M. Mirza, D. A. MacLaren, A. Samarelli, B. M. Holmes, H. Zhou, S. Thoms, D. MacIntyre, and D. J. Paul, "Determining the electronic performance limitations in top-down-fabricated si nanowires with mean widths down to 4 nm," Nano Lett. **14**, 6056–6060 (2014).
20. K. Biswas and S. Kal, "Etch characteristics of KOH, TMAH and dual doped TMAH for bulk micromachining of silicon," Microelectron J. **37**, 519–525 (2006).
21. G. G. Stoney, "The tension of metallic films deposited by electrolysis," Proc. Royal. Soc. London A: Maths. Phys. Char. **82**, 172–175 (1909).
22. E. Anastassakis, A. Pinczuk, E. Burstein, F. H. Pollak, M. Cardona, and R. Island, "Effect of static uniaxial stress on the Raman Spectrum of silicon," Solid State Commun. pp. 133–138.
23. D. Lockwood, *Light Scattering in Semiconductor Structures and Superlattices*, vol. 273 of *NATO ASI Series* (Springer US, 1991).
24. L. Shen, N. Healy, C. J. Mitchell, J. S. Penades, M. Nedeljkovic, G. Z. Mashanovich, and A. C. Peacock, "Mid-infrared all-optical modulation in low-loss germanium-on-silicon waveguides," Opt. Lett. **40**, 268–271 (2015).
25. Y. Sun, S. E. Thompson, and T. Nishida, "Physics of strain effects in semiconductors and metal-oxide-semiconductor field-effect transistors," J. Appl. Phys. **101**, 104503 (2007).
26. S. Birner, T. Zibold, T. Andlauer, T. Kubis, M. Sabathil, A. Trellakis, and P. Vogl, "Nextnano: General purpose 3-d simulations," IEEE Trans. Electron Dev. **54**, 2137–2142 (2007).
27. I. De Wolf, H. E. Maes, and S. K. Jones, "Stress measurements in silicon devices through Raman spectroscopy: Bridging the gap between theory and experiment," J. Appl. Physics **79**, 7148–7156 (1996).
28. M. Prost, M. E. Kurdi, A. Ghrib, S. Sauvage, X. Checoury, N. Zerounian, F. Aniel, G. Beaudoin, I. Sagnes, F. Boeuf, and P. Boucaud, "Tensile-strained germanium microdisk electroluminescence," Opt. Express **23**, 6722–6730 (2015).

1. Introduction

There has been significant interest in materials which are compatible with silicon foundry manufacture, such as strained Ge, that can be integrated into Si technology to allow expansion into new markets, such as Si photonics in the near-infrared (NIR) [1] and now the mid-infrared (MIR)[2, 3, 4] parts of the electromagnetic spectrum. With a direct bandgap only $\sim 140\,\text{meV}$ above the indirect valley [1], Ge has the potential to be an active CMOS compatible optical material [5]. Tensile strain has been demonstrated to decrease the difference between the direct and indirect bandgaps, enhancing the poor radiative recombination efficiency of the material by increasing the direct bandgap contribution. This approach has the potential to reduce the lasing thresholds in strained Ge lasers [6], compared to the optically and electrically pumped lasers previously demonstrated with low levels of tensile strain [7, 8]. The theoretical transition from indirect to direct bandgap is dependant on the choice of deformation potentials [1, 9], but is generally considered to be at $\sim 2\,\%$ biaxial strain.

GeSn devices have since demonstrated lasing with Fabry-Perot modes in waveguides [10]. Complex growth techniques, however, are required to incorporate sufficient Sn content into

#255977 Received 16 Dec 2015; revised 14 Feb 2016; accepted 14 Feb 2016; published 22 Feb 2016

GeSn direct bandgap alloys; while growth of Ge in Si foundries is now common place. Also, lasing in GeSn has yet to be demonstrated at room temperature so it is therefore still of interest to pursue a low threshold Ge laser device. Furthermore, in GeSn alloys, the Γ to L difference can also be further enhanced to increase the electron concentration at the Γ point, and therefore allow the potential for room temperature lasing. It is therefore beneficial to understand the nature of strain transfer into optical cavities, for engineering both Ge and GeSn material systems.

A number of methods for applying strain to Ge have been investigated. Early demonstrations used mechanically stressed membranes to investigate the limits of strain in small films [9]. Subsequently, high levels of strain have been demonstrated in micro bridge structures [11], and free standing membranes. Silicon nitride stressors have also been used to demonstrate high levels of strain in waveguides [12], pillar structures [13], and Ge micro-disks [14, 15].

The use of silicon nitride stressor layers is of interest due to the prior use of this technique in CMOS processes to strain Si channels, meaning strained Ge photonics could be easily integrated with electronics using standard processes. Micro-disks are of significant interest for Ge cavities, as they are compact resonators that allow for high strain transfer due to their undercut profile [14]. Furthermore, high Qs can potentially be achieved [16], which also serves to reduce the threshold for lasing. Highly strained Ge micro-disks have been demonstrated on GaAs substates [14], and using a double bonding technique to improve the strain uniformity in the vertical direction, which has been shown theoretically to improve gain [6].

This work demonstrates highly strained Ge on Si micro cavities, with single layer silicon nitride stressors. Micro-disk, micro-ring, and racetrack structures are demonstrated using a tetramethylammonium hydroxide (TMAH) wet etch, the anisotropy of which allows the fabrication of partially free standing structures. The highest strained cavities demonstrate in-plane, tensile strains of $> 2\,\%$ at the top surface, as measured by Raman spectroscopy and photoluminescence (PL) with up to 2.4 μm wavelength emission of light. Comparisons are made between the various cavity structures, which are discussed in terms of the impact of the geometry on the strain transfer, in-plane strain uniformity, and other aspects of the cavity design. Finally, the effect of shear strain around the circular cavities is discussed in terms of degradation of the carrier concentration at the Γ-valley, and alternative cavity structures without such problems are demonstrated. The improvements to the strain profile are confirmed using micro-Raman spectroscopy for analysis of the strain.

2. Growth and material properties

380 nm of Ge was grown on top of a Si (001) substrate in a Low–Energy–Plasma–Enhanced–Chemical–Vapour–Deposition (LEPECVD) tool at low temperatures of 500 ^{o}C, in order to avoid out-diffusion of degenerate phosphorus doping of 2.5×10^{19} cm^{-3} [17]. The activated dopant densities were measured using temperature dependent Hall bar measurements. This results in a Ge epilayer with negligible strain from growth, which was confirmed by Raman spectroscopy. High doping levels are advantageous in order to provide a strong PL signal, however in an optimised device, doping levels can be reduced to minimise free carrier absorption. This would also allow for high temperature anneals in order to reduce the threading dislocation density and induce a small, beneficial, tensile strain in the Ge layer from the mismatch in thermal expansion coefficients compared to the Si substrate.

3. Fabrication

Ge structures were patterned by electron beam lithography in a Vistec VB6 tool using using hydrogen silsesquioxane (HSQ) resist. The structures were subsequently dry etched in a mixed SF_6 and C_4F_8 recipe through to the Si layer, with an etch recipe which has previously

#255977 Received 16 Dec 2015; revised 14 Feb 2016; accepted 14 Feb 2016; published 22 Feb 2016

demonstrated low electrical [18, 19] and optical damage [4] to devices. A wet etch in tetramethylammonium hydroxide (TMAH) and isopropyl alcohol (IPA) was used to selectively etch the Si thereby undercutting the structures. The Si is etched anisotropically, giving the post shape observable in Fig. 1; the facets observed correspond to the $\{110\}$ and $\{111\}$ planes. The processing is simplified by the fact that the Ge layer can be used as the etch mask, due to the extremely high etch selectivities between Ge and Si. Furthermore, it should be noted that TMAH etching is compatible with processing in Si foundries [20]. A range of structures were fabricated using the above fabrication techniques, including micro-disk, micro-ring, and race-track structures. Arrays of 4, 5 and 6 μm diameter micro-disks and micro-rings were fabricated for PL measurements, and a number of larger micro-ring and race-track structures were included on such samples for analysis by Raman spectroscopy.

An interesting feature of the TMAH wet etch was found for larger ring structures. Due to the anisotropy of the wet etch, i.e, a selectivity of the (110) planes to the (111) planes, waveguide segments orientated parallel to different crystallographic directions are undercut at different rates. In fact this can lead to the full release of sections of the cavity, leaving support structures periodically around the structure, at regions parallel to the [110] directions, as demonstrated in Fig. 1(c).

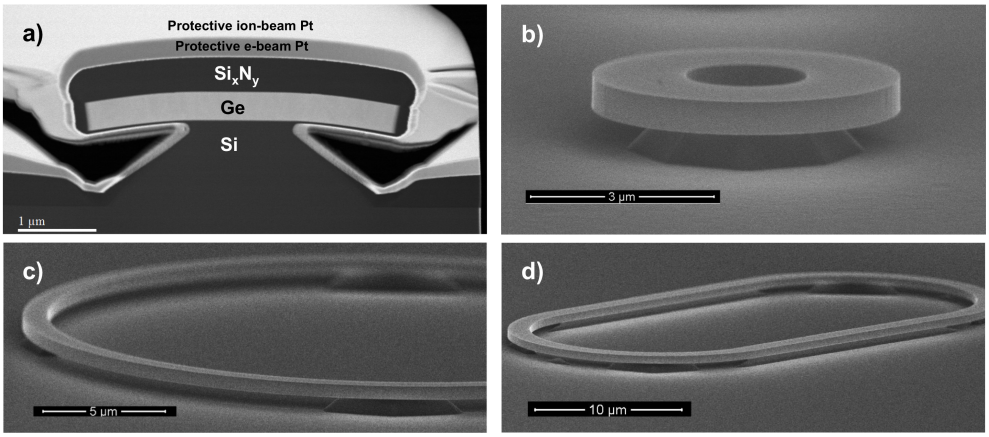

Fig. 1. (a) A cross sectional high angle annular dark field scanning transmission electron microscope image of a 4 μm diameter Ge micro-disk, after cross sectioning using a focussed ion beam microscope. (b) A scanning electron microscope (SEM) image of a 5 μm diameter Ge ring with a 1.5 μm waveguide width, which has been undercut by a wet etch. (c) A SEM of a 30 μm diameter ring structure undercut to produce free standing sections. (d) A SEM of a race-track cavity showing partially freestanding sections.

Following the wet etch step the structures were coated with high stress silicon nitride in an inductively coupled plasma enhanced chemical vapour deposition (ICP-PECVD) tool, which gives a high compressive stress of $\sim$2.4 GPa in the film when operated with an increased platen power. The control of stress with platen power is demonstrated in [13]. Exact stress values shall be given for each particular structure presented. Experimental stress values were calculated by measuring the curvature of a 100 mm Si wafer before and after silicon nitride deposition, using Stoney's equation [21], the details of which are discussed in [13]. A reference sample was fabricated with an undercut wet etch but with a silicon nitride film with negligible stress, which was used for photoluminescence (PL) and Raman spectroscopy measurements, to confirm the absence of significant heating from the laser. The silicon nitride film for this sample was deposited by operating the ICP tool with zero applied platen power, in a purely ICP mode.

#255977 Received 16 Dec 2015; revised 14 Feb 2016; accepted 14 Feb 2016; published 22 Feb 2016

4. Optical Characterisation

A Bruker Vertex 70 was used to measure the PL from strained Ge cavities. A ND:YAG emitting at 532 nm was used to pump micro-disk arrays with an unfocused spot. This would ensure low injection to minimise heating while producing a strong enough PL signal to be detected by the TE-InGaAs detector. The measurements were run in fast-scan mode and ambient blackbody radiation from heating could be observed towards the detector cut-off of 2.5 μm. Ambient room temperature blackbody measurements were taken and subtracted from the sample scans in order to observe photoluminescence. Due to a slight increase in the local temperature due to the laser heating, however, there is a differential heating tail observable in the measurements after subtraction of the ambient blackbody. This is observable in the PL in Fig. 2, particularly in the unstrained reference Fig. 2(a) from $\sim$ 2 to 2.5 μm , and similarly, in Figs. 2(b) and 2(c) for the 4 μm micro-disk and ring samples with no wet etch step (green curves).

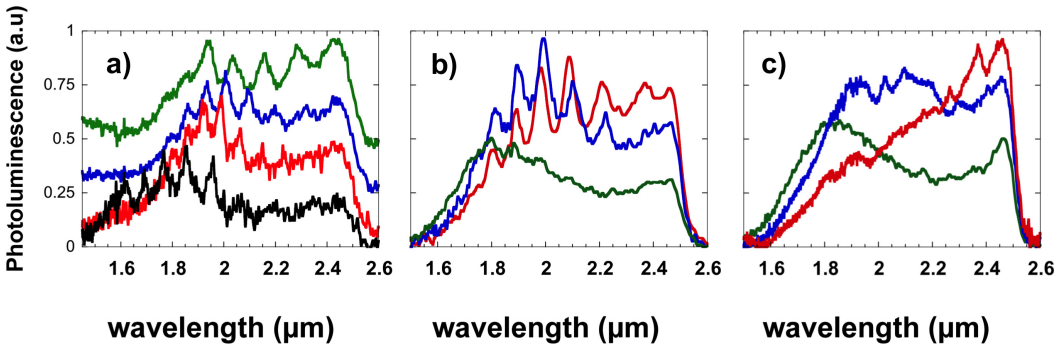

Fig. 2. (a) The photoluminescence (PL) from a 4 μm Ge micro-disks undercut by $\sim$ 1300 nm with no stress (black). Also shown is the PL from 4 μm (green), 5 μm (blue) and 6 μm (red) μm disks, undercut by $\sim$ 1300 nm with red-shifts induced by a 2.45 GPa silicon nitride stressor layer (b) 4 μm diameter Ge micro-disk with varying undercut. (c) 4 μm Ge diameter rings with 1.5 μm waveguide widths with varying undercut. For (b) and (c) the green curve demonstrate the samples with no wet etch, while the blue and red curves represent undercuts of $\sim$ 625 and 1250 nm respectively. The detector cut-off is $\sim$ 2.5 μm.

Clear resonances were visible for all micro-disks, which have been attributed to Fabry-Perot (FP) modes, Figs. 2(a) and 2(b). Ge squares with side lengths equal to the micro-disk diameters were patterned and PL measurements were taken, the observed resonances of which had a comparable free spectral range (FSR) to that of the micro-disks, therefore proving these are not whispering gallery modes (WGM). The modulation of the spectra by these resonances makes the identification of spectral peaks difficult. It would be expected, however, that no FP resonances should be observable below (above) the wavelength (energy) corresponding to the direct band transition, due to strong interband absorption. Transverse magnetic (TM) and transverse electric (TE) modes are supported in the micro-disk, which couple to Γ to light-hole (LH) and Γ to heavy-hole (HH) transitions respectively, at high levels of strain [1]. The resonance peak at the shortest wavelength should therefore give an indication of the Γ to HH interband transition, as otherwise TE modes below this wavelength could be supported, due to PL from lower strained regions of the micro-disk. This is only an approximation, however, as micro-disks of different diameter will have resonances at different spectral positions. Emission from 4, 5 and 6 μm disks, undercut by $\sim$ 1300 nm, with a 2.45 GPa silicon nitride stressor are presented in Fig. 2(a). An increasing red shift can be seen with decreasing diameter. This is observable as an increased attenuation of the resonances at shorter wavelengths (1.8 - 1.9 μm, and increased

#255977 Received 16 Dec 2015; revised 14 Feb 2016; accepted 14 Feb 2016; published 22 Feb 2016

emission intensity at longer wavelengths (2.2 - 2.4 μm). The measured PL suggests strain of $\sim$ 2 % in the 4 μm disks using the above arguments.

The trend of strain with varying undercut was subsequently investigated with the micro-disk and ring structures in Figs. 2(b) and 2(c). Three samples, each containing arrays of rings and micro-disks, of 4, 5 and 6 μm diameter were processed as described in the fabrication section; the first with no undercut (green), and the second and third with undercuts of $\sim$ 625 nm (blue) and $\sim$ 1250 nm (red) respectively. The ring structures have waveguide widths of 1.5 μm. Progressive increase in redshift can be observed with increasing undercut. The absence of Fabry-Perot modes in the ring geometry make the observation of spectral peaks possible, allowing another mechanism to quantify the levels of strain present in the cavity. From 4 μm rings with 1250 nm undercuts, there is a clear shift in the direct band emission, up to $\sim$ 2.4 μm, where emission at longer wavelengths is no longer visible due to the detector cut-off. This would be consistent with a tensile in-plane strain of $\sim$ 1.7 %, using deformation potentials reported in [9], assuming a Γ to LH transition.

A greater insight into the strain distributions is discussed in the following sections. As stated, with this optical setup, PL measurements have only been taken on the micro-disk arrays, rather than individual micro-disks. As a result no attempt will be made to analyse the Q factors of the observed resonances, as any finite difference in the cavities in the array would cause the resonances to broaden, leading to an inaccurate analysis of cavity losses. Furthermore, no whispering gallery modes could be observed with the surface normal collection of the emission.

5. Strain analysis

5.1. Raman spectroscopy

Raman spectroscopy can be used to calculate the local strain, in the volume set by approximately half the absorption depth of the excitation source, and the spatial resolution of the measurement [22]. Strain produces a shift in the phonon frequency, which in turn shifts the Raman line from the unstrained frequency. While this requires the assumption that the z-component of the strain is coupled to the in-plane strain by the relationship $\varepsilon_{zz} = -(C_{12}/C_{11})(\varepsilon_{xx}+\varepsilon_{yy})$, this can still provide useful insight into the strain distribution across the surface.

A WITec Alpha 300 RAS [13] was used to take confocal Raman maps of the strained micro-disks. A ND:YAG excitation source emitting at 532 nm was focused to a diffraction limited spot using an 100 $\times$ objective with a numerical aperture (NA) of 0.9. The absorption depth for this wavelength in Ge is $\sim$ 20 nm. Comparatively long integration times of 3 s per spectra allowed the laser power to be reduced to the point where heating is eliminated from the measurement, which was confirmed using the undercut, but unstrained reference sample. The 4 μm micro-disk with 2.45 GPa stressor, the PL of which was presented in Fig. 2(a), showed Raman shifts up to 291.1 rel. 1/cm, Fig. 3, which using a biaxial approximation, leads to in-plane, biaxial strains of $\sim$ 2.3%, when using Eq. 1, where C11 and C12 are the elastic constants of Ge, and p and q are the Raman deformation potentials reported in [23]. These simplify to give a strain shift coefficient of 424 cm^{-1}. This is consistent with the PL observed from these structures which indicated strain of $\sim$ 2 % based on deformation potentials [9]. Any slight discrepancy is consistent with the fact that strain gradients are expected in the vertical direction, as discussed in [14]. While the Raman measurement probes only the surface of the structure, it is expected that the PL should probe a larger volume due to carrier diffusion and the reduced self-absorption of the PL signal compared to the scattered Raman line.

$$\Delta\omega = \frac{(\varepsilon_{xx}+\varepsilon_{yy})}{2}\frac{1}{\omega_0}[-p\frac{C_{12}}{C_{11}}+q] \quad (1)$$

#255977 Received 16 Dec 2015; revised 14 Feb 2016; accepted 14 Feb 2016; published 22 Feb 2016

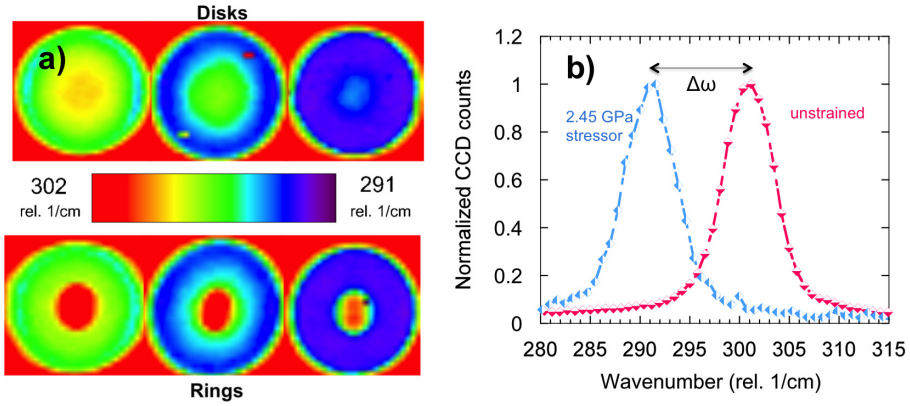

Fig. 3. (a) Raman maps of 4 μm micro-disks (top) and rings (bottom) with 300 nm thick, 2.37 GPa stressor layers. The structures on the left have no undercut etch, while at the centre and right they have undercuts of $\sim$625 nm and $\sim$1250 nm respectively. Each pixel is produced by fitting a Raman spectra with a single Lorentzian. The spectral position of the Lorentzian is then used to produce the colour map. (b) Raman spectra from a 4 μm micro-disk with a 2.45 GPa stressor showing a large shift of -9.9 1/cm. This corresponds to a strain of $\sim$ 2.3%

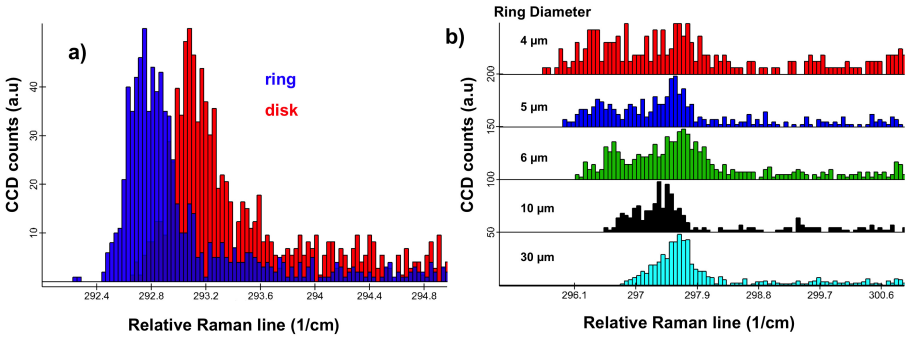

Fig. 4. (a) A histogram of the measured Raman line across a strained 6 μm diameter micro-disk and a ring cavity. The ring has a 1.5 μm waveguide width. Both structures had the same wet etch fabrication step and high stress silicon nitride layers. (b) Histograms for rings of varying diameter with no undercut and constant waveguide width of 1.5 μm. This demonstrates the trend of decreasing of the in-plane strain as the dimeter increases.

It was found in the ring geometry that the in-plane strain is more uniform than in micro-disks of an equivalent diameter. Furthermore, particularly with larger circumferences, the peak level of strain is larger in rings rather than micro-disks with equivalent processing. This is demonstrated in Fig. 4(a), which demonstrates histograms of the spectral position of the strained Raman line, for 6 μm diameter micro-disks and rings with identical wet etches and silicon nitride stressors (300 nm thick and 2.37 GPa). This is attributed to the reduced deformation resistance of the ring, with reduced lateral size compared to the micro-disks. Furthermore, there is a change in the undercutting profile when moving to larger circumference rings, as the wet etch from the inner circumference becomes more prominent, and regions of the ring become fully undercut.

Another benefit of the ring geometry is that it introduces another flexibility in the cavity

#255977 Received 16 Dec 2015; revised 14 Feb 2016; accepted 14 Feb 2016; published 22 Feb 2016

design. Cavities can be increased in diameter to reduce optical bending losses, and waveguide thicknesses can be chosen to give single mode operation. Furthermore, couplers could potentially be designed to couple to unstrained Ge bus waveguides, where emission above 2 μm can propagate with low loss [24]. Such structures were investigated with Raman spectroscopy. It was found that the relative Raman shift, and therefore the in-plane strain does reduce for increasing diameter, despite the constant waveguide width, Fig. 4(b). This is attributed to the fact that for small diameters, the stress transfer has a larger biaxial component, as the structure can be easily deformed in both x and y directions. For large diameters, the stress transfer is predominantly uniaxial in the direction transverse to the waveguide segment, similar to that in strained straight waveguides.

5.2. Finite Element Modelling

The strained Raman line reflects the in-plane strain, as demonstrated in Eq. 1. This, however, assumes zero shear strain, and therefore, finite element modelling (FEM) is required to provide further understanding of the strain distribution. COMSOL multiphysics was used to model the strain distribution in the 4 μm micro-disk, with the 2.45 GPa silicon nitride stressor. The model has the x and y directions orientated along the $\langle 100 \rangle$ crystallographic directions, and includes the anisotropy of the Ge elasticity tensor. Using the measured value of stress in the silicon nitride film was found to significantly underestimate the strain in the micro-disk. In order to accurately reproduce the experimental results, the modelled silicon nitride stress was increased until the vertical displacement of the micro-disk edge in the model, matched that measured by TEM in Fig. 1(a) (the vertical deflection at the micro-disk edge is $\sim$ 150 nm). The model demonstrates in-plane strains of 2.1 % at the top surface, which is in excellent agreement with the in-plane strains measured by Raman spectroscopy for this structure. These considerations confirm the self consistency of the modelled micro-disk.

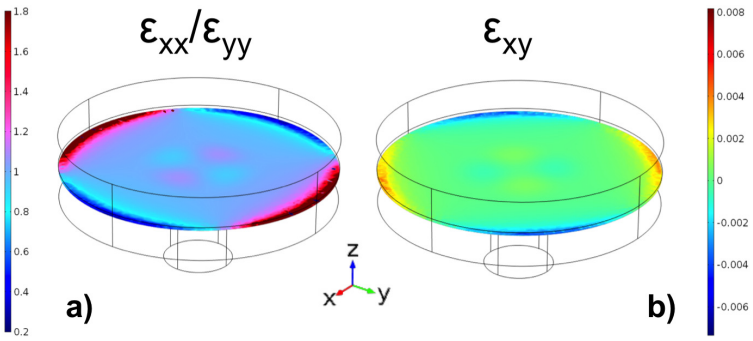

Fig. 5. COMSOL Multiphysics models of 4 μm Ge micro-disks with high stress silicon nitride layers. Both diagram present a 2D slice of a 3D model; the boundaries of which can be observed by the outline. The 2D slice is at the top of the Ge region. (a) demonstrates the ratio of ε_{xx} to ε_{yy}. (b) shows the shear strain, ε_{xy}, present at the edge of the micro-disk. The COMSOL model includes the anisotropy of the Ge elasticity tensor. x and y directions are orientated along the $\langle 100 \rangle$ crystal planes.

The nature of the transferred strain from a silicon nitride stressor to a Ge micro-disk is simulated in Fig. 5, where the $\varepsilon_{xx}/\varepsilon_{yy}$ ratio is shown. Large regions of the micro-disk top surface are biaxially strained, however towards the micro-disk edge, the stress transfer acts more uniaxially, in the radial direction. In the [100] direction, i.e. x and y directions, this stress transfer is clearly observed as uniaxial strain. In [110] directions, i.e. 45 ^{o} from x or y, the uniaxial stress

#255977 Received 16 Dec 2015; revised 14 Feb 2016; accepted 14 Feb 2016; published 22 Feb 2016

induces equal strains in ε_{xx} and ε_{yy}, but shear stresses are also induced, as demonstrated in Fig. 5(b).

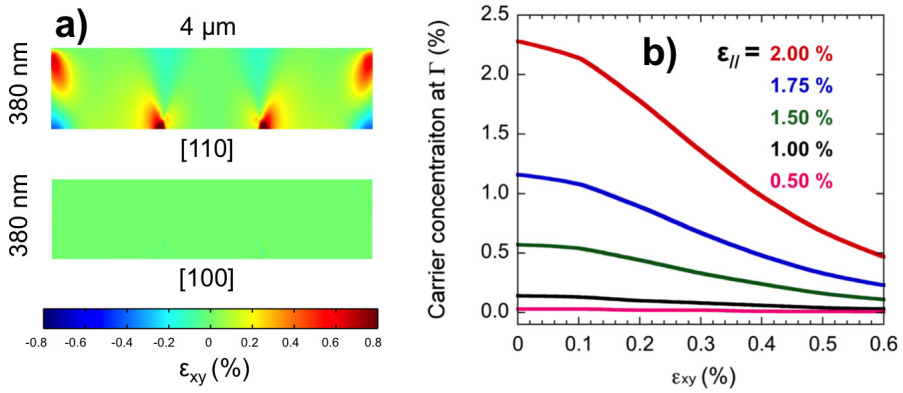

Fig. 6. (a) 2D slices from finite element models through a Ge micro-disk demonstrating the shear strain component ε_{xy}, orientated parallel to two different crystallographic directions. In the [110] direction, it can be observed that the uniaxial stress transfer induces shear strains at the micro-disk edge, while in the [100] direction the shear strains are close to zero. (b) The percentage electron concentration at the Γ band is shown as a function of the shear strain component ε_{xy}, for different levels of in-plane strain i.e. $(\varepsilon_{xx}+ \varepsilon_{yy})/2$. This demonstrates how the presence of shear strains can detrimentally effect the carrier concentration, and therefore the optical gain.

This was further examined by viewing the cross sectional plane parallel to the [110] direction in the model, and comparing it to an equivalent plane parallel to the [100] direction, where no ε_{xy} component of shear strain was present (see Fig. 6). It can be observed that in planes normal to the $\langle 110 \rangle$ directions, regions of shear strain extend inward to the micro-disk, predominantly with ε_{xy} values between $\sim$ 0.5 % and $\sim$ 0.3 % (the shear strains near the micro-disk centre have been ignored as whispering gallery modes will propagate nearer the micro-disk edge). This shearing of the Ge unit cell is known to remove the glide reflection plane of the crystal, which leads to splitting in the L valleys [25]. This serves to reduce the electron concentration at the Γ point, therefore reducing any potential gain that is available from regions strained in the [100] direction. The reduction in carrier concentration with increasing ε_{xy} shear component was calculated in Nextnano [26] for various levels of in-plane strain, Fig. 6(b). It can be observed that for a 2 % level of in-plane strain, a 0.4% shear strain results in a $\sim$ 57 % reduction in carrier concentration. Electron concentrations are calculated by Fermi-Dirac integrals, and the band structure has been calculated using an effective mass method, which does not take into account the non-parabolicity caused by strain. It should be noted, that this effect has been demonstrated experimentally in waveguides [12] with different orientations, but the presence of such strains in micro-disk and micro-ring geometries have not been considered in previous works, and has to be considered to fully understand the gain available from such cavities. The exact degradation of gain will of course require knowledge of the optical overlap of the mode with the strain distribution in the micro-disk. It was confirmed, by solving the Raman secular equation [27], that the levels of shear strains calculated for the 4 μm disk would give a negligible change to the Raman line, which is dominated by the in-plane components.

It was also found that the modelling confirmed the change from biaxial to uniaxial strain, in micro-rings of an increasing diameter with constant waveguide size. Further to this, it was found that this move to uniaxial strain increases the ε_{xy} shear component when the waveguide segment

#255977 Received 16 Dec 2015; revised 14 Feb 2016; accepted 14 Feb 2016; published 22 Feb 2016

lies in the $< 110 >$ directions. Therefore, micro-disk structures would still be favourable to micro-ring cavities with predominantly uniaxial strain.

The micro-rings can be designed such that the waveguide segments are orientated in the [100] direction, to form race-track structures as demonstrated in Fig. 1(d). It is convenient that the TMAH etch undercuts waveguide segments oriented in the [100] direction at a greater rate than in the [110], as this produces larger undercuts, or even free standing sections, which can be more easily strained. This is in the orientation where no ε_{xy} shear strains are present. Even with zero shear strain, however, the reduction of in-plane strain of the race-track would still suggest it is still beneficial to use a micro-disk structure if high levels of strain are required.

There are other advantages, however, of the undercut race-track structure, particularly if reduced levels of strain are required, for instance, in the GeSn material system. Race-track structures allow the possibility of leaving Si supports directly under the waveguide segments, as demonstrated in Fig. 1(d), which potentially provides improved heat-sinking of the device, or the means for electrical injection. This can still provide a cavity structure with no requirement for etching Bragg gratings, and the flexibility to control waveguide width for single mode operation. Conversely, while Ge micro-disks have increased strain, the electrical contacting appears limited to structures with full posts, as shown in [28], and it will likely be more difficult to electrically contact the device without disrupting the highly strained region.

6. Conclusion

Undercut Ge micro-cavities, including micro-disks, micro-rings, and race-track structures were fabricated using a combination of dry etching, and wet etching in TMAH. The wet etch step allows the Ge layer to act as the mask, and therefore simplifies the fabrication process. Furthermore, the anisotropy of the wet-etch allows the fabrication of partially free-standing structures. Undercut cavities were subsequently coated with a high stress silicon nitride layer in order to move the band-structure closer to a direct bandgap. In-plane strains of up to $\sim 2.3\%$ were measured in the highest strained cavities, which demonstrated photoluminescence at wavelengths upwards of 2.3 μm. The in-plane strain was then experimentally shown to increase with increasing undercut, by both Raman, and PL measurements, on both micro-disk and micro-ring cavities. Analysis of the in-plane strains by Raman spectroscopy gave an insight into the benefits of micro-ring structures, in terms of increased uniformity, and increased strain transfer at the top plane. Raman measurements also revealed the trend of biaxial to uniaxial stress transfer from small circumference (4 μm) to larger circumference (30 μm) micro-rings with constant waveguide size. Analysis of a micro-disk structure by finite element modelling demonstrated a uniaxial stress transfer in the radial direction at the micro-disk edge, which moves periodically from the [100] to the [110] directions. It was found that in the $< 110 >$ directions, ε_{xy} shear strains are induced with respect to the Ge unit cell, which serve to reduce the carrier concentration at the Γ-valley, and would therefore reduce available gain. Such effects are also present in micro-ring cavities. It is shown that race-track structures can be fabricated using identical processing techniques, with waveguide segments aligned to the $< 100 >$ directions to avoid shear strains. While these structures have reduced levels of strain, there are further advantages such as improved heat-sinking and ease of electrically contacting of strained cavities, which may be applicable to both Ge and GeSn material systems.

Acknowledgments

The authors would like to thank the staff of the James Watt Nanofabrication Centre for help with the fabrication. The work was funded by U.K. EPSRC (Project no. EP/N003225/1) and EC GEMINI (Project No. 613055).

#255977 Received 16 Dec 2015; revised 14 Feb 2016; accepted 14 Feb 2016; published 22 Feb 2016